Laminar Forced Convective Heat Transfer to Near-Critical Water in a Tube

Sang-Ho Lee*

Division of Mechanical System and Design Engineering, Wonkwang University, Iksan, Chonbuk 570-749, Korea

Numerical modeling is carried out to investigate forced convective heat transfer to near-critical water in developing laminar flow through a circular tube. Due to large variations of thermo-physical properties such as density, specific heat, viscosity, and thermal conductivity near thermodynamic critical point, heat transfer characteristics show quite different behavior compared with pure forced convection. With flow acceleration along the tube unusual behavior of heat transfer coefficient and friction factor occurs when the fluid enthalpy passes through pseudocritical point of pressure in the tube. There is also a transition behavior from liquid-like phase to gas-like phase in the developing region. Numerical results with constant heat flux boundary conditions are obtained for reduced pressures from 1.09 to 1.99. Graphical results for velocity, temperature, and heat transfer coefficient with Stanton number are presented and analyzed.

Key Words : Near-Critical Water, Convective Heat Transfer, Pseudocritical Point, Thermo-Physical Properties

Nomenclature

C_p : Specific heat at constant pressure (J/kg·K)
C_p^* : Nondimensional specific heat at constant pressure, $C_p/C_{p,in}$
D : Tube diameter (m)
f : Friction factor, $8\tau_w/\rho_{in}\cdot u_{in}^2$
h : Heat transfer coefficient (W/m²·K)
i : Enthalpy (J/kg)
k : Thermal conductivity (W/m·K)
L : Tube length (m)
Nu : Nusselt number, hD/k_b
P : Pressure (N/m²)
P_R : Reduced pressure, P/P_c
Pr : Prandtl number
Q : Heat flux (W/m²)
r : Radial coordinate (m)
Re : Reynolds number
St : Stanton number, $Q_w/\rho_b\cdot u_b\cdot(i_w-i_b)$
T : Temperature (K)
T_{pc} : Pseudocritical temperature (K)
T_R : Reduced temperature, T_{in}/T_c
T^* : Nondimensional temperature, $k_{in}(T-T_{in})/Q_w\cdot D$
u : Axial velocity (m/s)
u^* : Nondimensional axial velocity, u/u_{in}
V : Velocity vector (m/s)
v : Radial velocity (m/s)
z : Axial coordinate (m)

Greek Symbols

α : Grid non-uniformity parameter
β : Coefficient of thermal expansion (1/K)
ϕ : Dependent variable
μ : Dynamic viscosity (kg/s·m)
θ : Circumferential direction
ρ : Density (kg/m³)
ρ^* : Nondimensional density, ρ/ρ_{in}
τ : Shear stress (N/m²)
Φ : Viscous dissipation (J/kg·m²)

* **E-mail** : lsheagle@wonkwang.ac.kr
TEL : +82-63-850-6683; **FAX** : +82-63-850-6691
Division of Mechanical System and Design Engineering, Wonkwang University Iksan, Chonbuk 570-749, Korea.
(Manuscript **Received** November 28, 2002; **Revised** August 27, 2003)

Subscripts

b : Bulk condition
c : Critical point
in : Inlet
pc : Pseudocritical point
R : Reduced value
w : Wall

Superscript

it : Iteration

1. Introduction

Fluid flow and heat transfer to a fluid near the thermodynamic critical point are very complicated due to the large variation of thermodynamic and transport properties. The characteristics of momentum and heat transfer to fluid are coupled with the highly nonlinear variation of the properties, which makes flow phenomena more unpredictable compared with constant property case.

Figure 1 shows the properties variations of water for density, specific heat at constant pressure, viscosity, and thermal conductivity. When the fluid temperature is near the pseudocritical point at which specific heat is a maximum near the critical region at a specified pressure, phase transition like phenomena occur between liquid-like and gas-like behavior. Especially there is a peak in specific heat at constant pressure and thermal conductivity at this point. It may be expected that there is a relatively long relaxation time for a disturbed system to return to equilibrium state. As the system pressure approaches the critical point (T_c=647.07 K, P_c=22.05 MPa), the water properties variation is getting steeper near the pseudocritical point. Due to the large and nonlinear variations in the properties above but near the critical point it is quite difficult to predict the fluid flow and heat transfer phenomena.

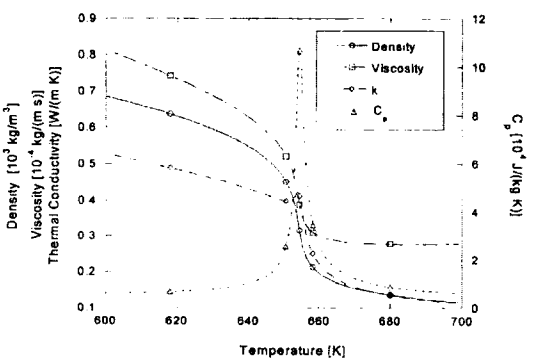

Fig. 1 Thermodynamic and transport properties of near-critical water at P=24 MPa

A lot of experimental and theoretical studies have been carried out to investigate the heat transfer phenomena near the critical point due to various applications such as power generation, missile rocket, and superconducter systems since 1950 (Hendricks and Simoneau, 1970; Hall, 1971; Polyakov, 1991). Due to the need for practical system design most studies are to investigate turbulent flow (Li et al., 1999; Olson, 1999), especially on the phenomena of heat transfer deterioration and improvement near the pseudocritical point (Shiralkar and Griffith, 1969; Kurganov and Kaptilnyi, 1993; Koshizuka et al., 1995). For laminar flow in a tube near the critical region, less research has been performed relatively. Koppel and Smith (1962) modeled the case of laminar flow in a tube for CO_2 near the critical region neglecting radial velocity component. Their results showed differences between constant property and near critical cases in the developing region of the tube. Dashevsky and Malkovsky (1985) also performed numerical investigation with boundary layer approximations using Boussinesq approximation. Vlakhov et al. (1981) suggested experimental heat transfer correlations for near-critical fluids in the laminar and transitional flow region. Zhou and Krishnan (1995) predicted laminar and turbulent heat transfer for channel flow for CO_2 near the critical point and compared their results with experimental data. Their results showed that the heat transfer rate could be lower for upward flow than for no-gravity flow in case of a constant wall temperature because turbulent viscosity is lower than that predicted for the no-gravity case. Despite the above several studies experimental data are still sparse and the effect of the properties variations on fluid flow and heat transfer near the critical region is not completely

understood.

In this study laminar forced convective heat transfer to water near the critical region in a tube is predicted by numerical modeling to investigate the momentum and heat transfer coupled with the large variations of thermodynamic and transport properties including proximity effect to the critical point.

2. Numerical Method

2.1 Numerical model

The problem to be analyzed is forced convective heat transfer to near-critical water flowing through a smooth walled circular tube with constant heat flux. Flow enters the tube with constant enthalpy and a fully developed velocity profile. The thermal resistance through and along the tube wall is neglected with the assumption of high thermal conductivity of the tube.

The flow is assumed to be axisymmetric and steady state with local thermodynamic equilibrium. The applicable governing equations of continuity, momentum, and energy are as following,

(a) Continuity :

$$\frac{1}{r}\frac{\partial}{\partial r}(\rho r v)+\frac{\partial}{\partial z}(\rho u)=0 \tag{1}$$

(b) Momentum :

$$\rho v\frac{\partial v}{\partial r}+\rho u\frac{\partial v}{\partial z}=-\frac{\partial P}{\partial r}+\frac{1}{r}\frac{\partial}{\partial r}(r\tau_{rr})-\frac{\tau_{\theta\theta}}{r}+\frac{\partial}{\partial z}(\tau_{rz}) \tag{2}$$

$$\rho v\frac{\partial u}{\partial r}+\rho u\frac{\partial u}{\partial z}=-\frac{\partial P}{\partial z}+\frac{1}{r}\frac{\partial}{\partial r}(r\tau_{rz})+\frac{\partial}{\partial z}(\tau_{zz}) \tag{3}$$

where

$$\begin{aligned}\tau_{rr}&=\mu\left[2\frac{\partial v}{\partial r}-\frac{2}{3}(\nabla\cdot V)\right]\\ \tau_{\theta\theta}&=\mu\left[2\frac{v}{r}-\frac{2}{3}(\nabla\cdot V)\right]\\ \tau_{zz}&=\mu\left[2\frac{\partial u}{\partial z}-\frac{2}{3}(\nabla\cdot V)\right]\\ \tau_{rz}&=\mu\left(\frac{\partial u}{\partial r}+\frac{\partial v}{\partial z}\right)\end{aligned} \tag{4}$$

(c) Energy :

$$\begin{aligned}\rho v\frac{\partial i}{\partial r}+\rho u\frac{\partial i}{\partial z}=&\left[\frac{1}{r}\frac{\partial}{\partial r}\left\{r\left(\frac{\mu}{\mathrm{Pr}}\frac{\partial i}{\partial r}\right)\right\}+\frac{\partial}{\partial z}\left(\frac{\mu}{\mathrm{Pr}}\frac{\partial i}{\partial z}\right)\right]\\ &-\left[\frac{1}{r}\frac{\partial}{\partial r}\left[r\left\{\frac{k(1-\beta T)}{\rho C_p}\frac{\partial P}{\partial r}\right\}\right]\right.\\ &\left.+\frac{\partial}{\partial z}\left\{\frac{k(1-\beta T)}{\rho C_p}\frac{\partial P}{\partial z}\right\}\right]\\ &+\left(v\frac{\partial P}{\partial r}+u\frac{\partial P}{\partial z}\right)+\mu\Phi\end{aligned} \tag{5}$$

As flow boundary conditions fully developed velocity and constant enthalpy are assumed at the inlet of the tube. Constant heat flux boundary condition is applied at the wall and symmetry condition is used at the centerline of the tube. At the outlet boundary of the tube, the dependent variables are linearly extrapolated to provide the axial downstream conditions. The outlet is placed 50-100 diameters downstream of the tube inlet.

In most modeling cases inlet water temperatures are below pseudocritical temperature at the specified inlet pressure. With heat flux from the tube wall water and wall temperatures increase gradually from along the tube. When the water temperature is near the pseudocritical temperature there is large variation in the water properties between the wall and centerline of the tube. All thermodynamic and transport properties of water are calculated with the computer code of Lester et al.(1984).

2.2 Solution procedure

The governing equations are solved with the SIMPLE algorithm using the second order upwind scheme. Convergence is checked by computing the normalized mass residual in the equation of continuity. Iteration is stopped when the residual is less than 10^{-3}. Successive iteration values of each variable should also satisfy the following convergence criteria,

$$\left|\frac{\phi^{it+1}-\phi^{it}}{\phi^{it}}\right|_{\max}<10^{-3} \tag{6}$$

where $\phi=u$, v, and i. For stability of convergence relaxation factors are used with values of 0.5-0.75 for velocities of u and v in the momentum equations, and for enthalpy in the energy

equation. All thermo-physical properties of water are also renewed iteratively with an relaxation factor (0.25-0.5).

For numerical calculation, orthogonal grid system that are axially and radially non-uniform is used. Following relations are used in the axial and radial grid system,

$$r=\frac{(\alpha_r+1)-(\alpha_r-1)\{[(\alpha_r+1)/(\alpha_r-1)]^{1-\bar{r}}\}}{[(\alpha_r+1)/(\alpha_r-1)]^{1-\bar{r}}+1} \quad (7)$$

$$z=\frac{(\alpha_z+1)-(\alpha_z-1)\{[(\alpha_z+1)/(\alpha_z-1)]^{1-\bar{z}}\}}{[(\alpha_z+1)/(\alpha_z-1)]^{1-\bar{z}}+1} \quad (8)$$

where $\bar{r}$, $\bar{z}$ are uniformly distributed grid systems. The non-uniform parameters of α_r and α_z are 1.5 and 1.2 respectively for axial and radial grid system to give enough grid points near the wall and entrance where there is large variation in heat transfer. For most of calculations with $L/D=100$ a grid of 300(600) $\times$75 (axial$\times$radial) is used. Grid dependence of the simulation results was checked by refining the axial and radial grid system and the effect of extrapolation boundary condition at the exit of the tube was checked by comparison with the results of longer tubes as shown in Fig. 2. All calculations were carried out on HP 1100 workstation with Compaq Fortran Compiler.

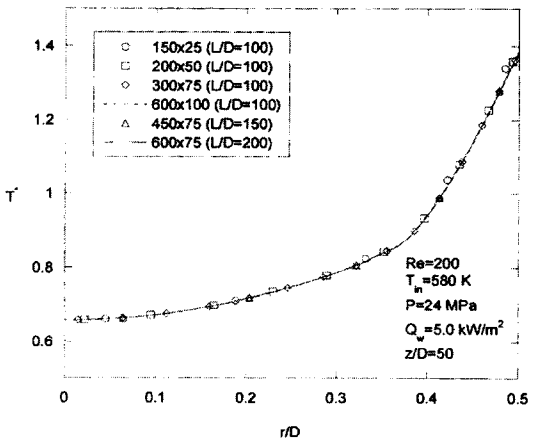

Fig. 2 Grid dependence and the effect of extrapolation boundary condition at the outlet of the tube

3. Results and Discussion

3.1 Comparison with other modeling

Current computations are compared with the results of Worsoe and Leppert (1965) for the variable property case to evaluate the accuracy of the developed code. Figure 3 shows the comparison of nondimensionalized axial velocity and temperature distributions in the entrance region of a tube. The definitions of parameters such as x^+, q^+, and Grashof number are the same as in Worsoe and Leppert (1965). The figure shows good agreement in the distributions of both velocity and temperature.

3.2 Distributions of fluid velocity, temperature, and properties in the tube

Figures 4 and 5 show developing axial velocity and temperature profiles at various downstream distances in a tube for inlet pressures of 24 MPa, 30 MPa, and 44 MPa. Water density and specific heat profiles are shown in Figs. 6 and 7.

Because of water density decrease by the heat transfer from the tube wall axial velocity at the centerline increases with z along the tube and the flow acceleration depends on the pressure in the tube. As the pressure in the tube approaches the

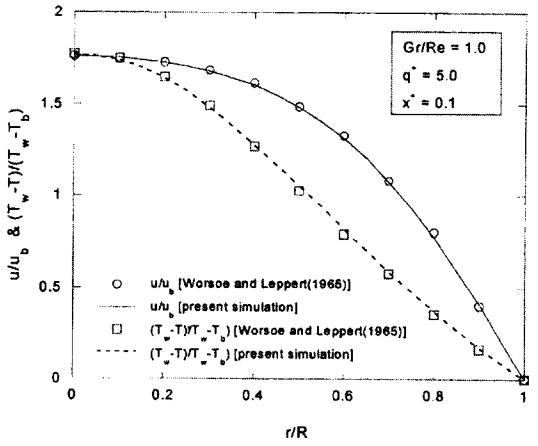

Fig. 3 Comparison of velocity and temperature distributions in the tube with the results of Worsoe and Leppert (1965) for variable property case

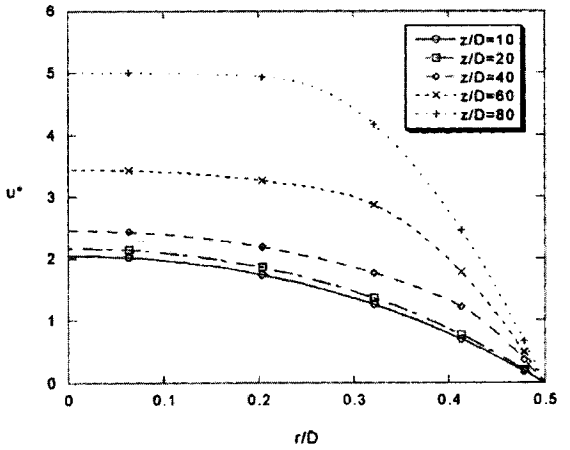

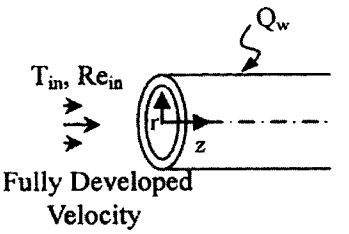

(a) 24 MPa (P_R=1.09)

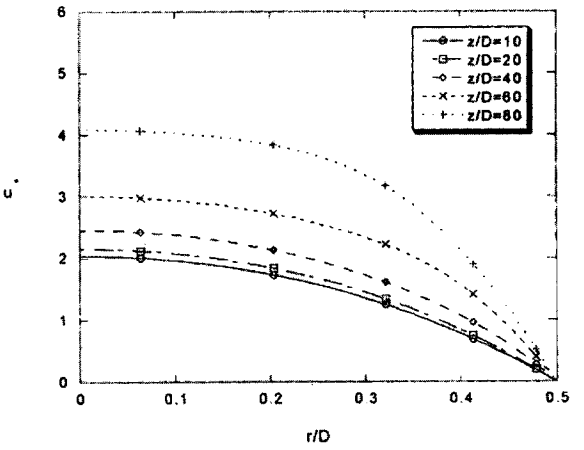

(b) 30 MPa (P_R=1.36)

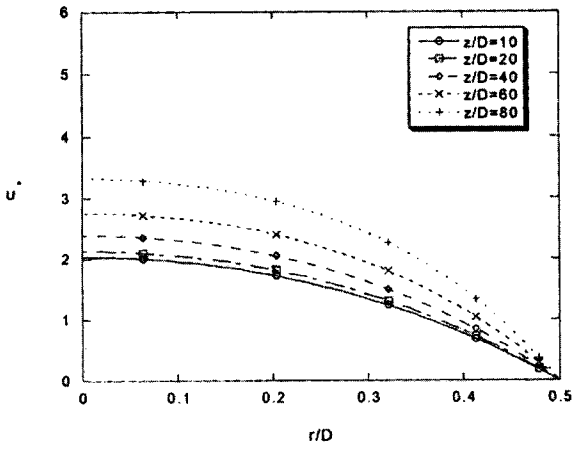

(c) 44 MPa (P_R=1.99)

Fig. 4 Radial profiles of axial velocity along the tube for various pressures in the tube at Q_w=5 kW/m^2, T_{in}=580 K, Re_{in}=200

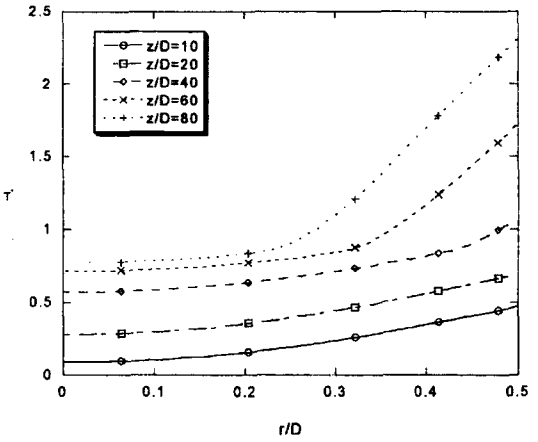

(a) 24 MPa (P_R=1.09)

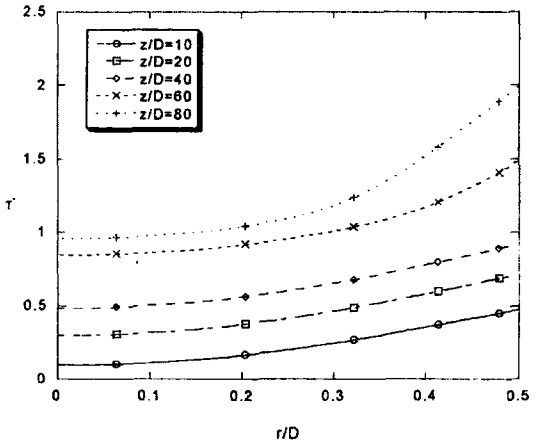

(b) 30 MPa (P_R=1.36)

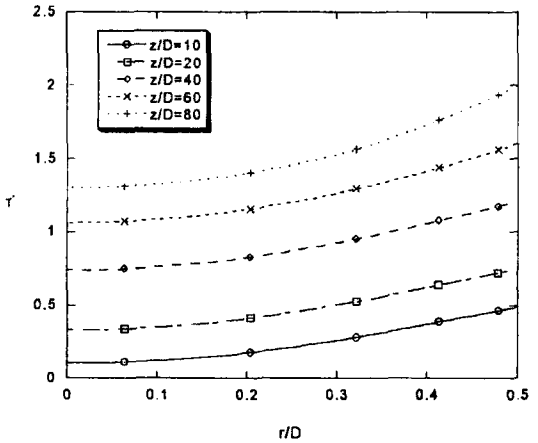

(c) 44 MPa (P_R=1.99)

Fig. 5 Radial profiles of temperature along the tube for various pressures in the tube at Q_w=5 kW/m^2, T_{in}=580 K, Re_{in}=200

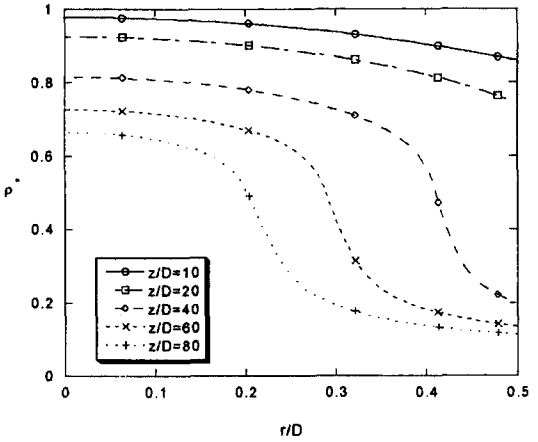

(a) 24 MPa (P_R=1.09)

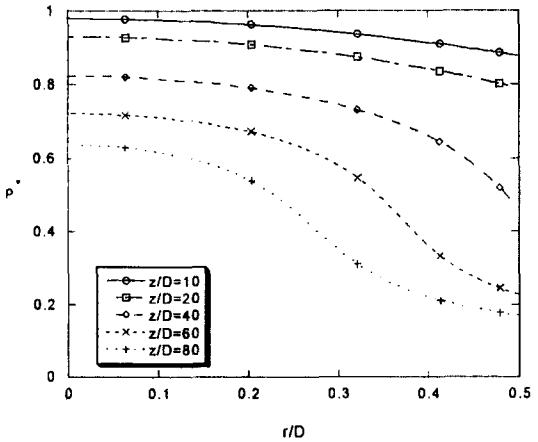

(b) 30 MPa (P_R=1.36)

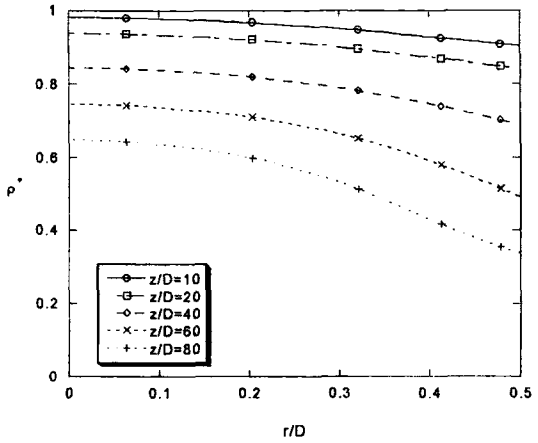

(c) 44 MPa (P_R=1.99)

Fig. 6 Radial profiles of density along the tube for various pressures in the tube at Q_w=5 kW/m^2, T_{in}=580 K, Re_{in}=200

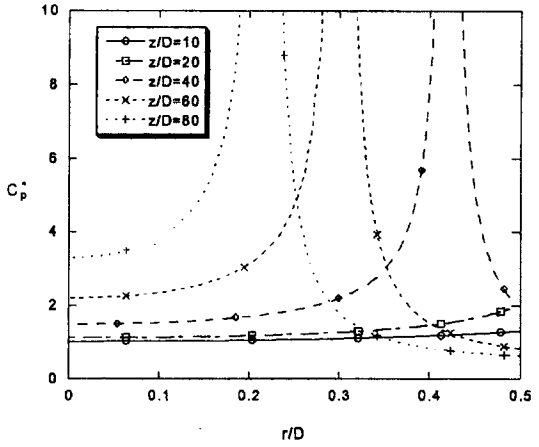

(a) 24 MPa (P_R=1.09)

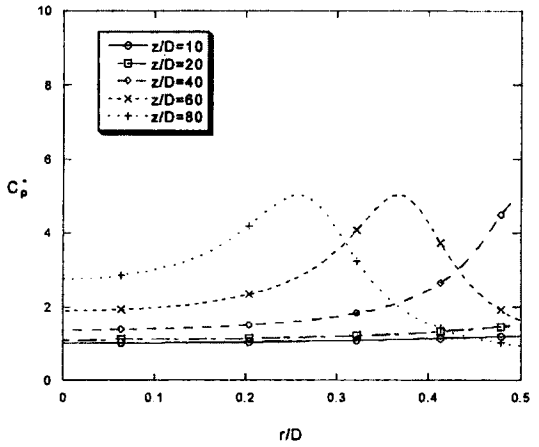

(b) 30 MPa (P_R=1.36)

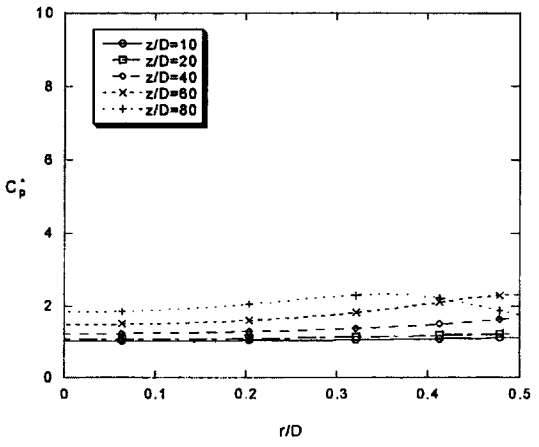

(c) 44 MPa (P_R=1.99)

Fig. 7 Radial profiles of specific heat along the tube for various pressures in the tube at Q_w=5 kW/m^2, T_{in}=580 K, Re_{in}=200

pressure of the critical point, centerline velocity increases more rapidly. It can also be seen that axial velocity gradient near the centerline becomes flatter with the decrease of pressure in the tube. When the fluid temperature is close to the pseudocritical temperature with steep variations in fluid properties, there is a change of radial temperature gradient across the tube. The temperature gradient in radial direction becomes steeper in the region where the fluid temperature is higher than the pseudocritical temperature, especially near the wall ($r/D>0.33$ at $z/D=60$ for $P=24$ MPa in Fig. 5). The temperature gradient change also increases as the pressure approaches the critical pressure. It is related with the steep decrease of thermal conductivity with temperature through the pseudocritical temperature as a transition from liquid-like phase to gas-like phase behavior.

As in Figs. 6 and 7 there are large variations of fluid density and specific heat across the tube section, and the pseudocritical temperature point of high specific heat moves radially toward the centerline. Although the fluid has severe variation of density and specific heat in the cross section of the tube, anomalous variations of the temperature profiles in the tube are relatively small, except temperature gradient. Again, phase change from gas-like behavior near the wall to liquid-like behavior in the core region can be seen in density distribution across the tube ($z/D>40$ for $P=24$ MPa in Fig. 6).

3.3 Effect of pressure and inlet temperature on heat transfer

Figure 8 shows heat transfer coefficient and Nusselt number distributions along the tube for various inlet pressures. The heat transfer coefficient decreases rapidly at the entrance and it begins to increase at a position ($z/D\approx20$ at P_R= 1.09) a little far from the entrance. The heat transfer coefficient goes through a maximum and then decreases again. This peak happens when pseudocritical temperature of pressure in the tube is higher than bulk temperature and less than wall temperature, especially closer to the wall temperature. It causes much larger specific heat near the

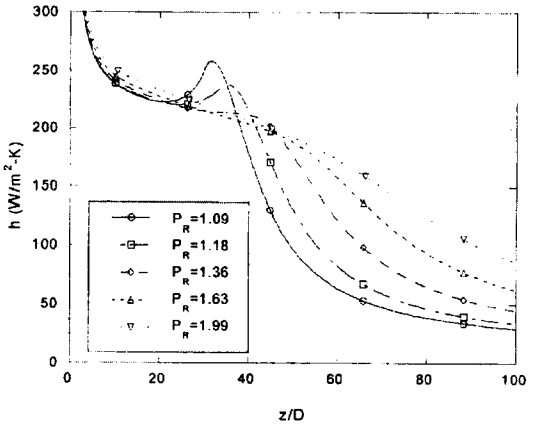

(a) Heat transfer coefficient

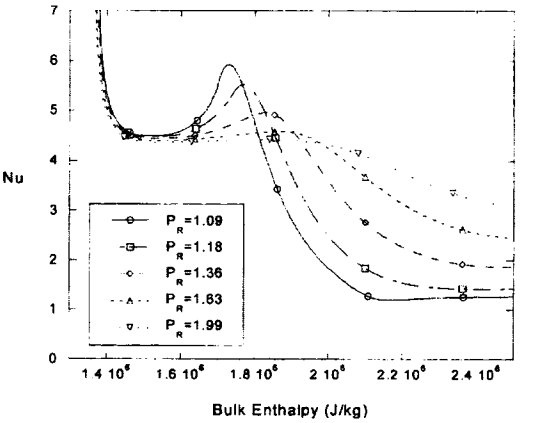

(b) Nusselt number

Fig. 8 Heat transfer coefficient and Nusselt number distributions for various pressures at Q_w=5 kW/m^2, T_{in}=580 K, Re_{in}=200

wall than that of the bulk fluid and convection mechanism dominates heat transfer rather than diffusion.

The peak in the heat transfer coefficient increases as the pressure approaches to the critical pressure because of the increase of maximum specific heat at the pseudocritical point with pressure. The axial position of the peak is moved downstream from the tube entrance due to the dependence of pseudocritical temperature on pressure. Table 1 shows pseudocritical temperatures and enthalpies for several pressures. As the pressure in the tube increases, the pseudocritical temperature increases almost linearly in the region of $1 < P_R < 1.36$.

Table 1 Pseudocritical temperatures and enthalpies of water for several pressures

P(MPa)	P_R	T_{pc}(K)	i_{pc}(kJ/kg)
24	1.09	654.4	2136.4
26	1.18	661.7	2165.1
30	1.36	675.5	2211.1
36	1.63	694.4	2264.6
44	1.99	715.4	2313.6

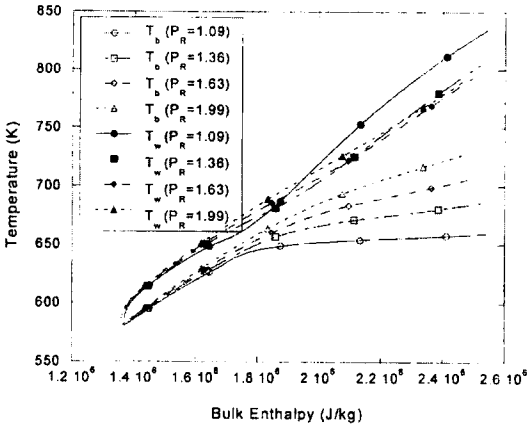

Fig. 9 Tube wall and bulk temperature distributions along the tube at Q_w=5 kW/m^2, T_{in}=580 K, Re_{in}=200

Figure 9 shows wall and bulk temperature distributions along the tube. Near the peak of the heat transfer coefficient the bulk temperature of water is lower than the pseudocritical temperature and the wall temperature is a little higher (T_b= 639 K, T_w=658 K for P_R=1.09 at the peak). The bulk temperature increases slowly near the pseudocritical temperature along the tube. The temperature difference between the wall and bulk fluid increases more rapidly through the peak as the pressure in the tube approaches critical point. It is because of the transition from the liquid-like phase to gas-like phase of water with the corresponding change of properties. Before T_b reaches T_{pc} the fluid has a characteristic of liquid and after T_b passes T_{pc} it has gas-like characteristic. With the increase of the temperature difference the heat transfer coefficient continuously decreases with z even though there is acceleration of water along the tube.

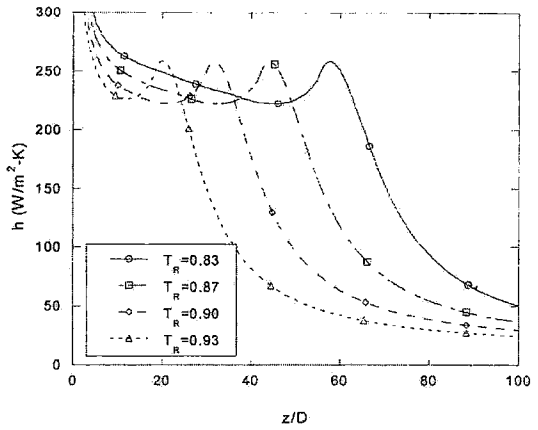

(a) Heat transfer coefficient

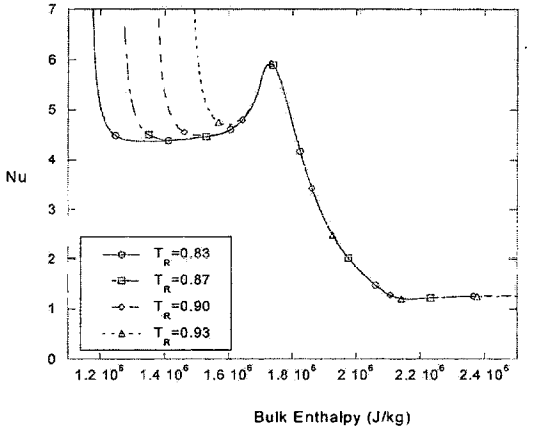

(b) Nusselt number

Fig. 10 Heat transfer coefficient and Nusselt number distributions for various inlet temperatures at Q_w=5 kW/m^2, P=24 MPa, Re_{in}=200

Figure 10 shows the heat transfer coefficient and the Nusselt number distributions for various inlet water temperatures. When water inlet temperature is lower than the pseudocritical temperature such as $T_R<1.01$, there is a peak in heat transfer coefficient distribution along the tube. It can be seen in the Nusselt number distributions along the tube that the peak of the heat transfer coefficient and corresponding bulk fluid enthalpy are influenced little by the water inlet temperature. If the inlet water temperature is higher than the pseudocritical temperature, there is no severe variation of properties and the heat transfer coefficient distribution is similar to constant property case.

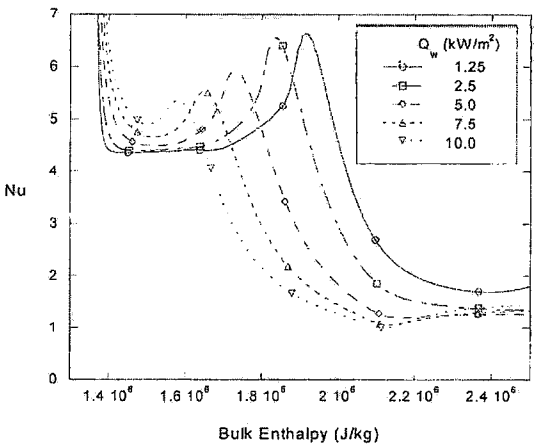

Fig. 11 Comparison of Nusselt number distributions for various wall heat fluxes at P=24 MPa, T_{in}=580 K, Re_{in}=200

Figure 11 shows the Nusselt number distributions for various wall heat fluxes. Peak of the Nusselt number decreases with the increase of heat flux from the tube wall. As the heat flux decreases the bulk enthalpy at the peak of the Nusselt number increases and it approaches the pseudocritical point (i_{pc}=2136.4 kJ/kg at P=24 MPa). This means that wall heat flux can affect the peak of the heat transfer coefficient even though pseudocritical enthalpy is not changed.

3.4 Stanton number and friction factor distributions

Near the critical region Stanton number is also an important parameter of the convection heat transfer because it includes the influence of variable properties. Figure 12 shows the Stanton number and friction factor distributions along the tube for various inlet pressures. As the bulk fluid enthalpy increases along the tube the Stanton number decreases in the entrance region and reaches a fully developed state without any peak near the pseudocritical point as in the heat transfer coefficient. The Stanton number decreases more rapidly as the pressure approaches the critical point. The fully developed Stanton number increases with the increase of pressure in the tube due to the properties variation. The Stanton number can be a useful parameter rather than heat

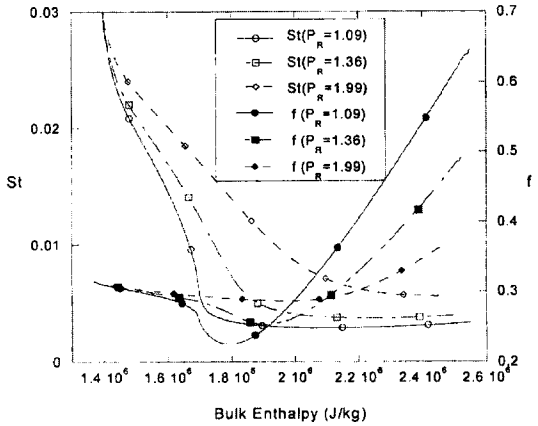

Fig. 12 Stanton number and friction factor distributions along the tube at $Q_w=5$ kW/m^2, $T_{in}=580$ K, $Re_{in}=200$

transfer coefficient or Nusselt number for the design of thermal systems which use near-critical fluids.

Friction factor decreases near the entrance and it reaches minimum near the pseudocritical point, and then it increases along the tube. This is caused by the flow acceleration and steep decrease of fluid viscosity near the pseudocritical point due to heat transfer. The minimum of the friction factor also decreases as the pressure approaches the critical point and the fluid bulk enthalpy of the minimum depends on the pseudocritical enthalpy.

4. Conclusions

Numerical calculations are performed for axisymmetric laminar forced convective heat transfer in the entrance region of a tube near the critical point for water. All thermo-physical property variations such as density, specific heat, viscosity, and thermal conductivity are included in the modeling. The large property variations near the critical region affect highly coupled fluid flow and heat transfer in the tube, especially close to the pseudocritical point. Following conclusions are found from the simulation results:

(1) Steep gradient of density produces rapid flow acceleration along the tube when there is a pseudocritical point in the tube.

(2) When bulk fluid enthalpy is close to the pseudocritical point there is a peak in the heat transfer coefficient distribution in the entrance region of the tube. Through the pseudocritical point of bulk fluid the heat transfer coefficient has a transition behavior along the tube between liquid-like phase and gas-like phase.

(3) The peak of the heat transfer coefficient increases as the pressure in the tube approaches critical point and wall heat flux decreases and it is influenced little by inlet fluid temperature.

(4) The Stanton number decreases along the tube as the bulk fluid enthalpy increases near the pseudocritical point without any peak as in the heat transfer coefficient. There is a minimum near the pseudocritical point in friction factor distribution and it becomes lower as pressure approaches the critical point.

Acknowledgment

This paper was supported by Wonkwang University in 2002.

References

Dashevsky, Y. M. and Malkovsky, V. I., 1985, "Heat Exchange with Laminar Upflow of Supercritical Helium in a Gravitational Field," *Cryogenics*, Vol. 25, pp. 658~659.

Hall, W. B., 1971, "Heat Transfer near the Critical Point," *Advances in Heat Transfer*, Vol. 7, pp. 1~83.

Hendricks, R. H. and Simoneau, R. V., 1970, "Survey of Heat Transfer to Near Critical Fluids," *NASA Technical Note*, NASA TN D-5886.

Koppel, L. B. and Smith, J. M., 1962, "Laminar Flow Heat Transfer for Variable Physical Properties," *Journal of Heat Transfer*, Vol. 84, No. 2, pp. 157~163.

Koshizuka, S., Takano, N. and Oka, Y., 1995, "Numerical Analysis of Deterioration Phenomena in Heat Transfer to Supercritical Water," *International Journal of Heat and Mass Transfer*, Vol. 38, No. 16, pp. 3077~3084.

Kurganov, V. A. and Kaptilnyi, A. G., 1993, "Flow Structure and Turbulent Transport of a

Supercritical Pressure Fluid in a Vertical Heated Tube under the Conditions of Mixed Convection Experimental Data," *International Journal of Heat and Mass Transfer*, Vol. 36, No. 13, pp. 3383~3392.

Lester, H., John, S. G. and George, S. K., 1984, *Steam Tables*, Hemisphere, New York.

Li, L. J., Lin, C. X. and Ebadian, M. A., 1999, "Turbulent Heat Transfer to Near-critical Water in a Heated Curved Pipe under the Conditions of Mixed Convection," *International Journal of Heat and Mass Transfer*, Vol. 42, No. 16, pp. 3147~3158.

Olson, D., 1999, "Heat Transfer in Supercritical Carbon Dioxide with Convective Boundary Conditions," *20th International Congress of Refrigeration*, IIR/IIF, Sydney, pp. 1~7.

Polyakov, A. J., 1991, "Heat Transfer under Supercritical Pressures," *Advances in Heat Transfer*, Vol. 21, pp. 1~50.

Shiralkar, B. S. and Griffith, P., 1969, "Deterioration in Heat Transfer to Fluids at Supercritical Pressure and High Heat Fluxes," *Journal of Heat Transfer*, Vol. 91, No. 1, pp. 27~36.

Vlakhov, E. S., Mieopol'skii, Z. L. and Khasanov-agaev, L. R., 1981, "Heat Transfer to a Supercritical Medium with Mixed Convection and Rising Flow in Heated Tubes," *Teploenergetika*, Vol. 28, No. 11, pp. 69~71.

Worsoe-Schmidt, P. M. and Leppert, G., 1965, "Heat Transfer and Friction for Laminar Flow of Gas in a Circular Tube at High Heating Rate," *International Journal of Heat and Mass Transfer*, Vol. 8, No. 10, pp. 1281~1301.

Zhou, N. and Krishnan, A., 1995, "Laminar and Turbulent Heat Transfer in Flow of Supercritical CO_2," *Proceedings of the 30th ASME National Heat Transfer Conference*, Portland, Vol. 5, pp. 53~63.